Strain engineering of the intrinsic spin Hall conductivity in a $SrTiO_3$ quantum well

Cüneyt Şahin,[1,*] Giovanni Vignale,[2] and Michael E. Flatté[1,†]
[1]*Optical Science and Technology Center and Department of Physics and Astronomy, University of Iowa, Iowa City, Iowa 52242, USA*
[2]*Department of Physics and Astronomy, University of Missouri, Columbia, Missouri 65211, USA*

(Received 1 April 2018; published 2 January 2019)

The intrinsic spin Hall conductivity of a two-dimensional gas confined to $SrTiO_3$, such as occurs at an $LaAlO_3/SrTiO_3$ interface, is calculated from the Kubo formula. The effect of strain in the [001] and the [111] directions is incorporated into a full tight-binding Hamiltonian for a quantum well with a [001] growth direction. We show that the spin-charge conversion ratio can be significantly altered through the strain and gate voltage by tuning the chemical potential. The strain direction is also a significant factor in the spin Hall response, as this direction affects the alignment of the conduction bands.

DOI: 10.1103/PhysRevMaterials.3.014401

I. INTRODUCTION

Two-dimensional electron gases (2DEGs) at oxide interfaces have attracted enormous interest due to their high carrier density and opportunities for control through atomic-scale interface engineering [1]. One of the most prominent examples is the *n*-type conducting interface of the perovskite insulators $LaAlO_3$ and $SrTiO_3$ [2] with high-density and high-mobility electrons. This system supports a rich spectrum of functionalities that can be accurately designed, tuned, and used in applications mainly due to the strongly correlated *d*-orbital electrons of titanium. Observed or predicted features include topological states at the $SrTiO_3$ surfaces [3], large Rashba coefficients, tunability by field effects and strain [4,5], metal-insulator transitions and multiferroicity [6,7], substantial spin-charge conversion [8,9], and adjustment of superconductivity by an applied gate voltage [10–12]. Furthermore, when the Rashba effect is suppressed, very long spin lifetimes have been predicted [13] and inferred from spin transport lengths of the order of several hundred nanometers [14] at room temperature.

The spin Hall effect describes the emergence of a perpendicular spin current in response to an external electric field in robust spin-orbit coupling systems [15–19]. The spin Hall conductivity (SHC) is the ratio of the spin current to the external electric field. This type of response may originate from different factors, including extrinsic effects such as skew scattering and side jump, but also may stem intrinsically from the band structure and Berry curvature of the Brillouin zone. Novel materials with giant SHC [20–22], as a result of the spin-orbit interaction, may be very useful in generating and controlling spin currents without external magnetic fields or ferromagnetic contacts. Additionally, strain may significantly influence the band structure, affecting the transport properties of the interfacial electron gas. The electron mobilities of $SrTiO_3$ can be enhanced up to 300% under compressive strain [23]. Strain may also alter the critical thickness of the $LaAlO_3$ required to form an electron gas [24], at the price of reducing the electric conductivity [25]. The charge carrier density and the localized magnetic moment at the interface [26], as well as the dielectric response [27] and the effective masses [28], are other strain-dependent properties. Therefore, realistic theories of such materials should consider epitaxial strain as a significant feature of the structure. There have been several attempts to measure spin-charge conversion ratios of these 2DEGs, with some impressive results, such as spin Hall angles between 0.15 [8] and 6.3 [29] at room temperature and high spin Hall angles with tunable Rashba coupling [9], which exceed the spin Hall angles of materials such as Pt [30], Ta [31], and III–V semiconductors [32]. A robust spin-galvanic effect exhibiting a sign change has been predicted [33] within a minimal three-band model. Giant spin-orbit torques, spin accumulation [34], and Fermi energy-dependent spin responses [35] are expected as a result of Rashba spin-orbit interactions [36]. This large body of work suggests a significant spin-dependent response to electric fields in these systems. However, the intrinsic spin Hall conductivity due to atomic spin-orbit interactions has not been studied in detail, especially considering the effects of epitaxial and external strains on the intrinsic SHC.

Here we calculate the intrinsic SHC for a strained two-dimensional (2D) electron gas at the $LaAlO_3/SrTiO_3$ interface from the Kubo formula by a full Slater-Koster tight-binding Hamiltonian. This atomistic approach enables a full Brillouin zone calculation of the SHC, thus improving upon perturbative calculations based on $\mathbf{k}\cdot\mathbf{p}$ models. Tight-binding Hamiltonians require a small number of parameters and result in far shorter computational times than typical for *ab initio* computations. The effective strain along the [001] and [111] directions enters into the Hamiltonian through modified overlap integrals according to bond angles and bond lengths following Harrison's law, which states that overlap integrals change by the square of the ratio of unstrained to strained bond length, i.e., $H_{\mathrm{hop}} \propto (d_{\mathrm{unstr}}/d_{\mathrm{str}})^2$. The intrinsic SHC of these systems is highly sensitive to the chemical potential and also to the strength and direction of the strain, offering opportunities for performance enhancement through strain engineering.

*cuneytsahin@mailaps.org
†michael_flatte@mailaps.org

II. FORMALISM

A. Intrinsic spin Hall conductivity

The intrinsic SHC is a result of an interplay between the details of the band structure, the strength of the spin-orbit interaction, the chemical potential, and the direction of the current relative to crystal axes [15,37–39]. For a system with an electric field oriented along $\hat{x}$, the spin current is directed along $\hat{y}$, and the spin direction along $\hat{z}$. The spin Hall conductivity can be evaluated from the Kubo formula as a spin current–electric current response function in the clean static limit [22,40]

$$\sigma_{yx}^{z} = \frac{e\hbar}{V}\sum_{\mathbf{k}}\sum_{n} f_{\mathbf{k}n}\Omega_{n}^{z}(\mathbf{k}), \tag{1}$$

where V is the volume of the system, $f_{\mathbf{k}n}$ is the Fermi-Dirac distribution function, and the "Berry curvature" $\Omega_{n}^{z}(\mathbf{k})$ is

$$\Omega_{n}^{z}(\mathbf{k}) = \sum_{n\neq n'} 2\mathrm{Im}\frac{\langle u_{n\mathbf{k}}|\hat{j}_{y}^{z}|u_{n'\mathbf{k}}\rangle\langle u_{n'\mathbf{k}}|\hat{v}_{x}|u_{n\mathbf{k}}\rangle}{(E_{n\mathbf{k}}-E_{n'\mathbf{k}})^{2}}. \tag{2}$$

The spin current operator and components of the velocity operator, $\hat{j}_{y}^{z}$ and $\hat{v}_{i}$, are

$$\hat{j}_{y}^{z} = \frac{\hbar}{4}(\hat{v}_{y}\sigma_{z}+\sigma_{z}\hat{v}_{y}) \quad \text{and} \quad \hat{v}_{i} = \frac{1}{\hbar}\nabla_{k_i}\hat{H}. \tag{3}$$

Note that $\Omega_{n}^{z}(\mathbf{k})$, as defined above, is not a Berry curvature in the strict sense, since the spin current cannot be rigorously expressed as the derivative of the Hamiltonian with respect to a Bloch wave vector. Instead $\hat{j}_{y}^{z}$ is the derivative of the Hamiltonian with respect to a spin-dependent vector potential. Nevertheless, Eq. (1) is exact, as it follows from the Kubo formula. In what follows, we continue to refer to $\Omega_{n}^{z}(\mathbf{k})$ loosely as a "Berry curvature," and we describe its structure as a function of the Bloch wave vector and energy. It is useful to rewrite Eq. (1) so that the chemical potential dependence is captured efficiently by introducing the density of curvatures $\rho_{\mathrm{doc}}(\epsilon)$, which is the contribution of the Berry curvature per unit energy. Introducing the energy-dependent Fermi function $f(\epsilon)$ yields

$$\sigma_{yx}^{z} = \frac{e\hbar}{A}\int d\epsilon\rho_{\mathrm{doc}}(\epsilon)f(\epsilon), \tag{4}$$

where A is the area of the 2D system. This quantity, the density of the Berry curvature, $\rho_{\mathrm{doc}}(\epsilon)$, allows one to interpret the sources of the spin Hall conductivity and its dependence on the temperature, external effects such as strain, and the chemical potential. Equations (1), (2), and (4) suggest that a Hamiltonian which captures wave functions, energies, and curvatures of the system is required to compute the intrinsic SHC.

B. Strained tight-binding Hamiltonian

Both $LaAlO_3$ and $SrTiO_3$ have cubic symmetry and belong to the O_h^1 space group [41]. A plot of a simple cubic perovskite crystal and its Brillouin zone is shown in Fig. 1. The existence of both inversion and time-reversal symmetry results in doubly degenerate bands, different from III–V semiconductors and their heterostructures. To get an accurate picture of the wave functions and energies in Eq. (2) we rely on a low-energy effective Hamiltonian that is constructed using a Slater-Koster tight-binding model [42] with nearest-neighbor

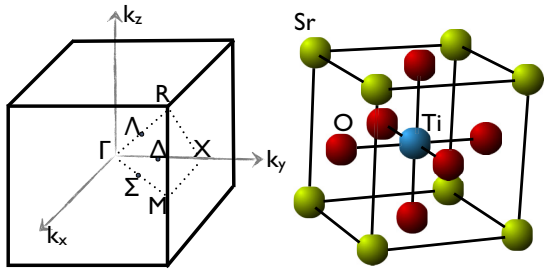

FIG. 1. Reciprocal lattice and crystal structure of a typical perovskite oxide with the general formula ABO_3. Atom B (titanium in this case) is connected to six oxygen atoms, forming an octahedron. Atom A at the corners (strontium) usually contributes its s electrons that are at high energies. The oxygens' p orbitals constitute the valence band. The itinerant d orbitals of atom B form the conduction band and determine most of the transport properties of n-type systems.

interactions. Starting with an atomic orbital $\phi_{n}(\mathbf{r}-\mathbf{R}_{i})$ at the atomic position $\mathbf{R}_{i}$, the Bloch sum of these atomic orbitals is

$$\psi_{n}(\mathbf{r}) = \sum_{\mathbf{R}_i} e^{i\mathbf{k}\cdot\mathbf{R}_i}\phi_{n}(\mathbf{r}-\mathbf{R}_{i}). \tag{5}$$

The tight-binding Hamiltonian is then calculated by summing over the nearest neighbors at $\mathbf{R}_{j}$:

$$\hat{H}_{mn} = \sum_{\mathbf{R}_i} e^{i\mathbf{k}\cdot(\mathbf{R}_j-\mathbf{R}_i)}\int \psi_{n}^{*}(\mathbf{r}-\mathbf{R}_{i})H\psi_{m}(\mathbf{r}-\mathbf{R}_{j})d\mathbf{r}. \tag{6}$$

The first expression above is the phase factor depending on the relative distances between atoms in the crystals, whereas the integral (also called the overlap integral) depends on the bond angles and bond lengths. Strain produces two significant changes to the tight-binding Hamiltonian in Eq. (6). First, it changes atomic distances in the crystal, thus altering the strength of the overlap integrals and phase factors. Second, changes in the bond angles may induce further two-center Slater-Koster integrals that were not present in the original Hamiltonian due to symmetry. The former is integrated into the unstrained Hamiltonian via Harrison's scaling law [43], which alters the strength of the interaction in proportion to the bond length and the inverse square rule (d^{-2} rule). The latter is incorporated in the Hamiltonian by changing the directional cosines. For instance, three primitive lattice vectors of perovskite oxides are $\mathbf{a}_{i} = \frac{a}{2}\hat{i}$ and six oxygen atoms around the titanium are located at $\pm\mathbf{a}_{i}$, where i stands for x, y, or z, and a is the lattice constant as shown in Fig. 1. For a symmetric general strain ϵ_{ij}, oxygens in Fig. 1 move to

$$\begin{aligned}\mathbf{a}_{1}' &= \frac{a}{2}(\epsilon_{xx}+1,\epsilon_{xy},\epsilon_{xz}),\\ \mathbf{a}_{2}' &= \frac{a}{2}(\epsilon_{yx},\epsilon_{yy}+1,\epsilon_{yz}),\\ \mathbf{a}_{3}' &= \frac{a}{2}(\epsilon_{zx},\epsilon_{zy},\epsilon_{zz}+1),\end{aligned} \tag{7}$$

whereas titanium's position remains unchanged at the center. The distance between titanium and oxygen atoms changes from $d = a/2$ to

$$d_{i}' = \frac{a}{2}\sqrt{(1+\epsilon_{ii})^{2}+\epsilon_{ij}^{2}+\epsilon_{ik}^{2}}. \tag{8}$$

In the case of a small strain, this distance changes to $a/2(1+\epsilon_{ii})$ and the volume of one unit cell changes from Ω_0 to $\Omega' = \Omega_0(1+Tr(\epsilon))$. Without any deformation due to strain, a typical Hamiltonian matrix element between a d_{xy} orbital of titanium and a p_x orbital of the second oxygen is

$$H_{d_{xy},p_x} = 2i\sin\left(\frac{a}{2}k_y\right)(pd\pi), \tag{9}$$

where $(pd\pi)$ refers to the overlap matrix element in a π-bond configuration. This matrix element transforms under a general strain to

$$H_{d_{xy},p_x} = \left[\frac{\sqrt{3}\epsilon_{yx}^2(1+\epsilon_{yy})}{\left(\epsilon_{yx}^2+(1+\epsilon_{yy})^2+\epsilon_{yz}^2\right)^{3/2}}pd\sigma' + \frac{(1+\epsilon_{yy})\,(1-2\epsilon_{yx}^2)}{\left(\epsilon_{yx}^2+(1+\epsilon_{yy})^2+\epsilon_{yz}^2\right)^{3/2}}pd\pi'\right] \times 2i\sin\left(\frac{a}{2}(k_x\epsilon_{xy}+k_y(\epsilon_{yy}+1)+k_z\epsilon_{yz})\right), \tag{10}$$

where $pd\pi' = pd\pi/(1+2\epsilon_{yy})$ and $pd\sigma' = pd\sigma/(1+2\epsilon_{yy})$ are scaled overlap integrals (for small strain). Equation (10) can be further simplified for small strain, as second-order terms can be neglected. As expected this expression approaches Eq. (9) as the strain approaches 0. The other off-diagonal elements of the Hamiltonian have been constructed and studied as a function of the strain in a similar fashion.

C. Spin-orbit coupling and interfacial quantum confinement

We have also added the intrinsic spin-orbit Hamiltonian, obtained by computing atomic spin-orbit couplings from atomic spectra using the Landé interval rule. The basis of a tight-binding Hamiltonian needs to be doubled once the spin-orbit coupling is introduced. The Hamiltonian with spin takes the form

$$H = \begin{pmatrix} H_{\rm tb} & 0 \\ 0 & H_{\rm tb}\end{pmatrix} + H_{\rm so},$$

where $H_{\rm so} = \lambda_i \mathbf{L}\cdot\mathbf{S}$ in the Russell-Saunders coupling scheme. The form of the spin-orbit Hamiltonian for p, d, and f orbitals has been published [44]. Here $\mathbf{L}$ is the orbital angular momentum operator, $\mathbf{S}$ is the spin operator, and λ_i is the strength of the renormalized atomic spin-orbit coupling. This value is related to the atomic spin-orbit couplings, ξ_i. λ_i differs for p and d orbitals, λ_p and λ_d, and vanishes for s orbitals so $\lambda_s = 0$. The atomic spin-orbit coupling depends on the particular configuration of the p or d electrons [45]. For a given atomic ground-state configuration a standard term symbol has the form ${}^{2S+1}X_J$, where S is the total spin, J is the total angular momentum, and X is a letter depending on L such that it is S for $L=0$, P for $L=1$, D for $L=2$, etc. [46]. The value of the atomic spin-orbit coupling can be calculated from the Landé interval rule, in other words, from the energy difference for the specific term symbol, which is tabulated [47] as

$$\xi_i = \frac{E(J)-E(J-1)}{J}, \tag{11}$$

where the index i represents p or d orbitals. When more than two J exist one will get multiple ξ_i for each splitting. Since the resulting energy intervals are very close to each other we considered the average ξ as the value of the spin-orbit coupling. The relation between the spin-orbit coupling λ and the atomic spin-orbit coupling ξ is obtained through the total spin S, such that $\lambda_i = 2S\xi_i$. The splitting of the energy levels in a crystal can be expressed in terms of the splitting of the spectral lines of atoms as

$$\Delta_0 = \frac{E(J)-E(J-1)}{J}\times(2S)\times\frac{2L+1}{2}\times C_N, \tag{12}$$

where C_N is a normalization factor that is 1 for row 2 elements and 1.56 for row 3 elements, e.g., for oxygen and titanium, respectively [48]. This factor is required for several reasons. First, neither valence nor conduction band edges are formed from pure p or d orbitals and both include higher-order atomic orbitals. Second, Wannier functions of atomic orbitals tend to extend more than the typical size of the Wigner-Seitz cell, which causes a volume effect [48]. For instance, the ground state of the carbon is ${}^3P_0$ with $S=P=1$ with three energy levels and term symbols ${}^3P_0$, ${}^3P_1$, and ${}^3P_2$, respectively. The energy difference $E(J)-E(J-1)$ is measured as 16 $\rm cm^{-1}$ [47], therefore the atomic spin-orbit coupling from Eq. (11) gives $\xi_p = 2$ meV, and $\lambda_p = 2S\times 2$ meV $= 4$ meV. The resulting splitting of valence band energies in the crystal is then $\Delta_0 = 4$ meV $\times (2L+1)/2 = 6$ meV, which agrees excellently with the experimental splitting. Similarly, we calculate the spin-orbit couplings as $\lambda_p = 15.2$ meV for oxygen and $\lambda_d = 20.1$ meV for titanium from the atomic spectra. Consequently, this leads to a splitting of the bands by about 30 meV, consistent with the experimental values.

Finally, for epitaxially grown strontium titanate films an interfacial quantum confinement effect (H_i) has a significant influence on the conduction bands. The total Hamiltonian of our model becomes

$$H_{\rm tot} = H_{\rm tb}^{\rm str} + H_{\rm so} + H_i, \tag{13}$$

where $H_{\rm tb}^{\rm str}$, $H_{\rm so}$, and H_i are the strained tight-binding, the spin-orbit, and the interfacial quantum confinement terms, respectively. The atomic spin-orbit interactions and quantum confinement effects are especially relevant, as they alter the band structures and band degeneracies substantially. Electronic states of $SrTiO_3$ in the vicinity of the conduction band minimum (Brillouin zone center) consist of d orbitals of titanium.

Here we focus on the six t_{2g} quantum well states (three orbital and two spin states) of a [001]-oriented quantum well, with the lowest quantum well wave function quantum number $n=1$. For an infinitely wide quantum well there is a spin-orbit splitting of about 30 meV between a fourfold multiplet and a doublet. Additional interfacial or quantum well confinement breaks the fourfold degeneracy by shifting the energies of the d orbitals along $\hat{z}$, so that d_{yz} and d_{zx} have different energies than d_{xy}. The existence of three doubly degenerate conduction subbands, well split from a higher ladder of subband states, has been reported both for $LaAlO_3/SrTiO_3$ interfaces [49] and for bulk $SrTiO_3$ surfaces [50] for (001)- and (111)-oriented samples, respectively. A further detailed review [51] also indicates the formation of

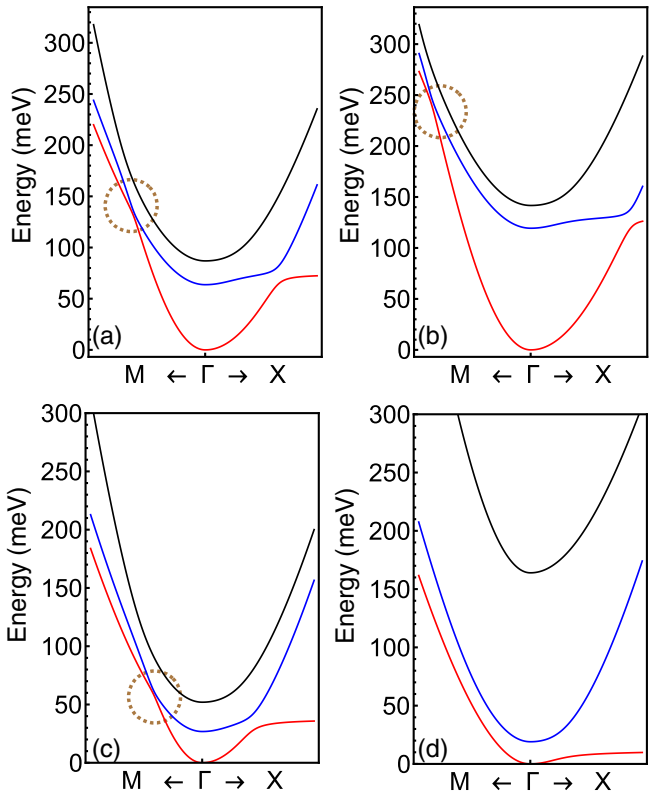

FIG. 2. Electronic structure of the lowest three conduction bands (a) for a tensile strain of 1.5% along the [001] direction, (b) for a compressive strain of −1.5% along the [001] direction, (c) for a tensile strain of 0.4% along the [111] direction, and (d) for a compressive strain of 1.5% along the [111] direction. The Brillouin zone points where bands nearly touch are circled.

subbands due to the confinement potential and increase in the subband separation as the width is decreased. In this work, we assume that the width of the quantum well, which is always oriented along [001], is sufficiently thin that the first three (doubly degenerate) conduction subbands, which dominate the intrinsic SHC, can be separately examined, since all other subbands are at higher energies as a result of the confinement potential and the strain. An energetic separation of 100 meV from the confinement potential corresponds to a quantum well width of approximately 3 unit cells, in agreement with our thin-well picture.

In Fig. 2 we summarize the 2D band structure of our system for various strains in various directions by plotting the first three conduction bands. In general, the strain shifts certain bands with respect to others depending on the strain direction, which we discuss in Sec. III.

III. RESULTS AND DISCUSSION

A. Stress along [001]—the growth direction

We first need to address the effect of strain on diagonal matrix elements within the tight-binding Hamiltonian, which correspond to the on-site energies. In contrast to the off-diagonal elements of the Hamiltonian, on-site matrix elements have neither directional factors nor overlap integrals (unless further nearest neighbors are added). Strain, however, changes the symmetry of the crystal and, as a result, can either increase or decrease on-site energies depending on the direction of the strain. For instance, stress along the [001] growth direction induces a biaxial strain and lowers the group symmetry from O_h to its subgroup D_{4h} (nonsymmorphic space group D_{4h}^{18}). The same reduction of the point-group symmetry occurs when the temperature is decreased below 100 K [52] and the crystal structure makes a transition from the cubic to the tetragonal phase. Consequently, results at temperatures higher than 100 K with strain are similar in symmetry to those at low-temperature without strain. The on-site energy shift depends on the magnitude of the strain tensor.

The relation between strain and stress is determined by the components of the compliance tensor,

$$\epsilon_{ij} = \sum_{k,l} S_{ijkl}\sigma_{kl}, \tag{14}$$

which is a rank 4 tensor but can be greatly simplified for cubic crystals. For a uniaxial stress along the [001] direction, the stress and strain tensors are related to each other such that

$$\sigma = \begin{pmatrix} 0 & 0 & 0 \\ 0 & 0 & 0 \\ 0 & 0 & 1 \end{pmatrix}, \quad \epsilon = \begin{pmatrix} s_{12} & 0 & 0 \\ 0 & s_{12} & 0 \\ 0 & 0 & s_{11} \end{pmatrix}. \tag{15}$$

The relevant elastic constants of the compliance tensor for this study, s_{11}, s_{12}, and s_{44} (for stress along [111]) are reported in the literature [53]. Our terminology for 1% strain means that a stress is applied to generate $\epsilon_{zz} = 1\%$ along the axis of the stress, and the other strain elements are determined according to force-free boundary conditions on the other surfaces, which follow from the elastic constants, so $\epsilon_{xx} = \epsilon_{yy} = s_{12}/s_{11} \times 1\%$. The conduction bands of $SrTiO_3$ at the zone center with t_{2g} symmetry are analogous to the valence bands of zinc-blende crystals with a heavy electron, a light electron, and a split-off bands. Therefore, for a stress along the epitaxial growth direction [001], strain acts as a tetragonal crystal distortion and, thus, as a perturbation with Γ_{12} symmetry. The threefold degenerate conduction bands of the strontium with $\Gamma_{25'}$ symmetry will split into doubly degenerate Γ_5^+ and singly degenerate Γ_4^+ of the D_h group. Therefore this results in shifting the energy of E_{yz} and E_{zx} with respect to E_{xy} by $3E_{001}$, where

$$E_{001} = 2b(\epsilon_{zz} - \epsilon_{xx}) \tag{16}$$

and b is the tetragonal deformation potential. The constant b (d in the case of strain along [111]) is calculated to be −0.51 eV (−2.15 eV) [54]. Our calculations of the response of the band edges under tensile and compressive strains are in excellent agreement with previous *ab initio* calculations [54,55].

Once we introduce the strain along [001] into the tight-binding Hamiltonian by shifting the on-site energies and modifying the directional cosines and overlap integrals, then we calculate and plot the intrinsic SHC of the $LaAlO_3/SrTiO_3$ 2DEG with different configurations in Fig. 3. In this configuration, the potential associated with the confinement of electrons is taken as 100 meV. This would be a reasonable estimate since a confinement potential below 30 meV is not adequate to form a 2D electron gas, as d electrons would be

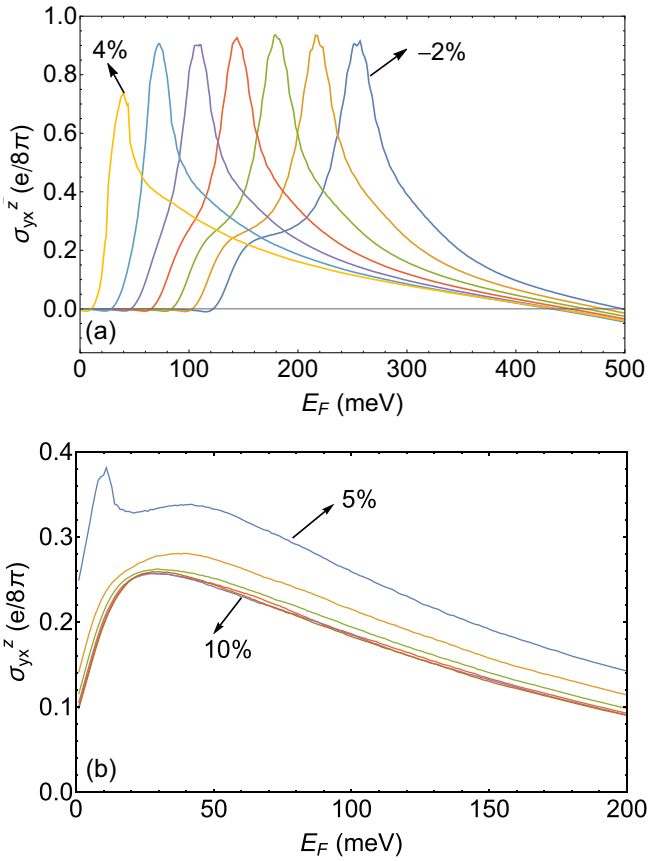

FIG. 3. Intrinsic SHC as a function of the Fermi level in $LaAlO_3/SrTiO_3$ 2DEGs (a) for increasing strain on the growth direction [001], from a compressive −2% to a tensile 4%, and (b) for a much higher tensile strain, from 5% to 10%, both by an increment of 1%. The zero of the energy corresponds to the conduction band edge at the Γ point and the confinement potential is taken to be 100 meV.

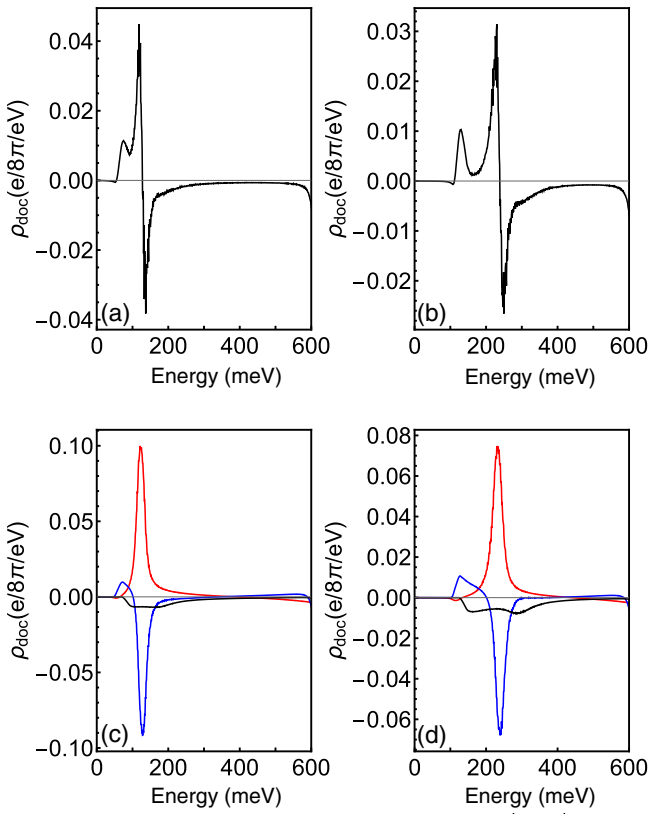

FIG. 4. (a) Density of curvatures for a tensile strain of 1.5%, (b) density of curvatures for a compressive strain of −1.5%, (c) band-resolved contribution to the Berry curvatures for the case in (a), and (d) band-resolved curvature contribution for (b). Red, blue, and black curves represent the first, the second, and the third conduction bands in Fig. 2, respectively.

lost into the bulk [56]. Comparison with the electronic band structure, density of curvatures and the SHC calculations leads us to several observations. First, the contribution from the lowest conduction band is much smaller than that from higher bands until the Fermi level starts to introduce carriers in the second conduction band. The energy difference between the conduction subbands is large when E_F lies at the conduction band edge, due to the large band gap (3.2 eV) and the splitting of these conduction subbands due to strain, the confinement potential, and the spin-orbit coupling. The lowest conduction subband contribution to the SHC is negative for small Fermi energies, leading to a slightly negative SHC up to the Fermi level, whereupon the second band starts to contribute, which suggests that there is a carrier density threshold beyond which the SHC changes sign. This sign change originates from the fact that negative and positive curvature densities exist at energetically different k points. Although strain does not change the energy difference between the second and the third bands substantially at the zone center, a compressive strain shifts the first subband away from the higher two subbands, and tensile strain decreases the gap between the two. The positive Berry curvature of the second subband therefore contributes at lower Fermi levels for tensile strain, as shown in Fig. 3.

The maximum SHC occurs when the Fermi level crosses the nearly touching first and second bands for strain along [100], as shown in Figs. 2(a) and 2(b). These close band crossings, which are depicted by brown circles, act as sources of very large Berry curvature, and therefore they determine the carrier density at which the highest SHC would be observed. Passing through the crossing point, the sign of the Berry curvature is reversed, and as a consequence, the SHC decreases as the Fermi level is further increased.

This result can be understood better by investigating the band structure and distribution of the Berry curvature [Figs. 4(a) and 4(b)] within the Brillouin zone. The band-resolved density-of-curvature plots provide more insight into this behavior. As shown in Figs. 4(c) and 4(d), the first conduction band makes an initially negative but in general positive contribution to the SHC, whereas the third band provides negative curvature at all energies. The second conduction band determines the characteristics of the SHC curve. Initially, the second band contributes positive curvatures at low energies. As the chemical potential increases, the contribution of the second band decreases and becomes negative, reaching a magnitude identical to the first band's maximum. The offset in the energies where these maximum and minimum curvatures are located results in the features seen in the total SHC. Comparing different strains [such as

1.5% in Figs. 4(a) and 4(c) vs −1/5% in Figs. 4(b) and 4(d)] leads to the conclusion that shifting the bands with strain shifts the chemical potential at which the maximal SHC occurs.

We also calculated the SHC for carrier densities that vary from 1.5×10^{14} to 6×10^{14} cm $^{-2}$, corresponding to moving the Fermi level from 90 to 300 meV. These densities, which are achievable through doping or gate voltage, are in excellent agreement with previous experiments on strained $LaAlO_3/SrTiO_3$ 2DEGs [26]. Our calculations are also in agreement with the observation that the uniaxial tensile strain greatly enhances the carrier density [57]. Another effect of strain in this direction is the tetragonal deformation of the octahedral structure consisting of six oxygens. This deformation leads to a rotation angle. The distance between titanium and the oxygens in the xy plane $d_\parallel = a_\parallel/\cos(\pi - \alpha)$, where $\pi/2 - \alpha$ is the angle along Ti-O-Ti. This angle is exactly $\pi/2$ without strain, corresponding to a completely straight line along the Ti-O-Ti direction. However, this angle changes with tensile strain, whereas the out-of-plane distance between titanium and oxygen ($d_\perp$) increases and the in-plane distance ($d_\parallel$) decreases. This results in a rotation which can be expressed in terms of strain elements as $\alpha = \cos^{-1}[1/(s_{11}/s_{12} \times \epsilon_{zz} + 1)]$. For a strain of 1.4% this effect results in a rotation of 4.6°, which is in excellent agreement with the experimentally measured value of 4.58° in a 2DEG of 300-unit-cell $SrTiO_3$ thickness [25].

B. Strain along [111]

Applying strain along [111] vs [001] differs, as the strain affects a different diagonal element of the Hamiltonian. A uniaxial stress along [111], where $\sigma_{ij} = 1$, results in the strain tensor

$$\epsilon = \frac{1}{3}\begin{pmatrix} s_{11} + 2s_{12} & s_{44}/2 & s_{44}/2 \\ s_{44}/2 & s_{11} + 2s_{12} & s_{44}/2 \\ s_{44}/2 & s_{44}/2 & s_{11} + 2s_{12} \end{pmatrix}. \quad (17)$$

Here 1% strain indicates $\epsilon_{xx} = \epsilon_{yy} = \epsilon_{zz} = 1\%$. Other elements of the tensor are calculated via compliance tensor elements. This type of strain acts as a perturbation with Γ_{15} symmetry which shifts E_{xy} by E_{111}, where

$$E_{111} = 2\sqrt{3}d\epsilon_{xy}, \quad (18)$$

and d is the trigonal (or rhombehedral) deformation potential. Our calculations of strained band structures are in excellent agreement with previous *ab initio* computations [54].

A negative strain pushes bands away from each other and the SHC is nearly 0 until the doping is increased to the point where the chemical potential crosses to the second conduction band. This high doping would be a difficult doping level to achieve. At the zone center, however, a positive [111] strain moves the d_{xy} band closer to the upper energy levels (differently from [001] quantum wells, where the d_{xy} subband is separated from the higher bands). This would close the gap from the interfacial potential between the first subband and the higher subbands. In the case of positive strain, we observe two distinct behaviors. For very low strain, from 0 to 0.5%, our results resemble those for strain along the [001] direction, i.e., increasing strain causes bands to move closer

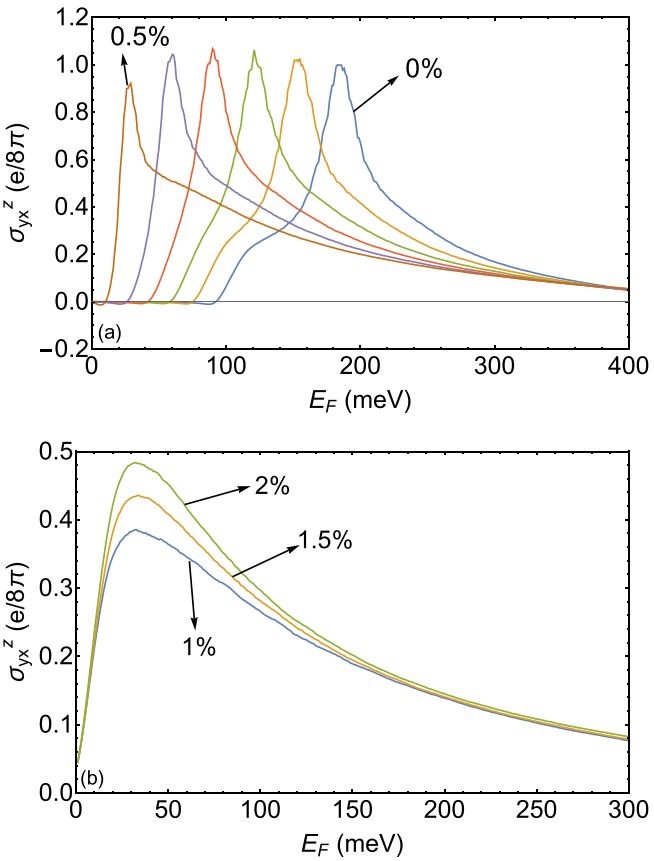

FIG. 5. Intrinsic SHC as a function of the Fermi level in $LaAlO_3/SrTiO_3$ (001) oriented 2DEGs strained along the [111] direction. (a) Tensile strain from 0% to 0.5%, increasing by an increment of 0.1%; (b) tensile strain of 1%, 1.5%, and 2%. The energy is measured from the conduction band edge at the Γ point. The confinement potential is taken as 100 meV.

and the chemical potential of the maximum SHC is also shifted towards the band edge.

The resulting spin Hall conductivity is shown in Fig. 5. However, once the lowest conduction band is increased to the level of the second conduction band and forms a degenerate state at about 0.5% strain, the overall shape of the SHC changes. As increasing strain increases the separation between bands, we observe a behavior similar to that shown in Fig. 3(b). One significant difference is that increasing strain increases the spin Hall conductivity. This can be explained readily by computing the curvature of the third band, which is negative. Increasing strain results in a larger separation between the first two bands and the third band; thus, the negative curvature of that band has less impact on the overall spin Hall conductivity (Fig. 6). Band-resolved density-of-curvature plots [Figs. 6(c) and 6(d)] indicate that for values of the strain up to 0.5% the evolution is similar to what was found for strain in the [001] direction. The first band has primarily positive curvature, and the second band has mostly negative curvature but shifted in energy slightly with respect to the first band, which results in a threshold chemical potential at which the density of curvature changes sign, thus creating a maximum SHC. This threshold Fermi level is about 70 meV above the band edge and corresponds to a doping level with a

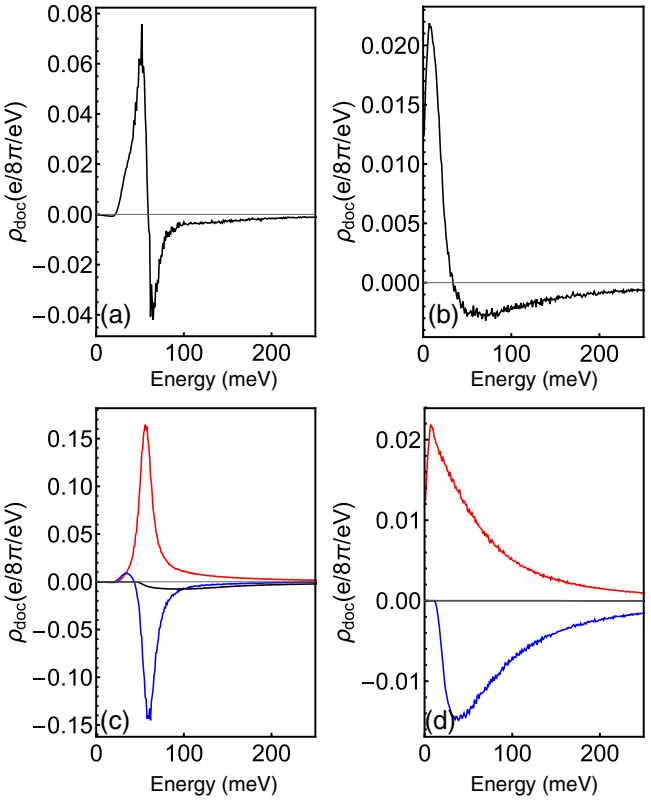

FIG. 6. (a) Density of curvatures for a tensile strain of 0.4% along the [111] direction, (b) density of curvatures for a compressive strain of 1.5%, (c) band-resolved contribution to the Berry curvatures for the case in (a), and (d) band-resolved curvature contribution for (b). Red, blue, and black curves represent the first, the second, and the third conduction bands, respectively.

carrier density of 1.7×10^{15} cm^{-2}. In the case of 1.5% strain, the third band is shifted so far away that it does not contribute to SHC for achievable chemical potentials. The first band and second band contributions compete with each other, as the positive first band has a slightly lower energy than the second band. In this case, the threshold Fermi level is in between the first two conduction bands (≈40 meV) and corresponds to a carrier density of 1.5×10^{14} cm^{-2}. These carrier densities are in the experimental range.

C. Temperature dependence

We set the temperature to 0 K for the calculations in the previous sections. The intrinsic nature of the spin-orbit-dependent phenomena does not depend on the temperature; however, the Fermi-Dirac distribution in Eq. (1) contains the effect of the temperature indirectly so that the temperature dependence can be obtained through the occupation function. We would like also to note that Boltzmann transport theory [58] for these materials does not apply to this calculation, as the intrinsic spin Hall conductivity is a property of the filled valence states at all energies and does not depend on the quasiparticle features or scattering at the Fermi energy. The temperature effectively acts as a broadening in the occupation function. We plot the temperature dependence of the intrinsic SHC in Fig. 7 for a tensile strain of 1% along the [001] direction. The SHC exhibits a similar behavior at different temperatures, and the maximum of the SHC is located at the same Fermi energy. The increase in the intrinsic SHC can be observed up to the maximum SHC, however, the magnitudes are smaller than the value at zero temperature. The decrease in the scale is attributed to the broadening of the occupations such that negative Berry curvatures after 150 meV in Fig. 4(a) contribute to the total spin Hall conductivity at lower Fermi levels as the temperature is increased. Although the effect is decreased, it is still of the same order of magnitude as at zero temperature and, thus, observable in experiments.

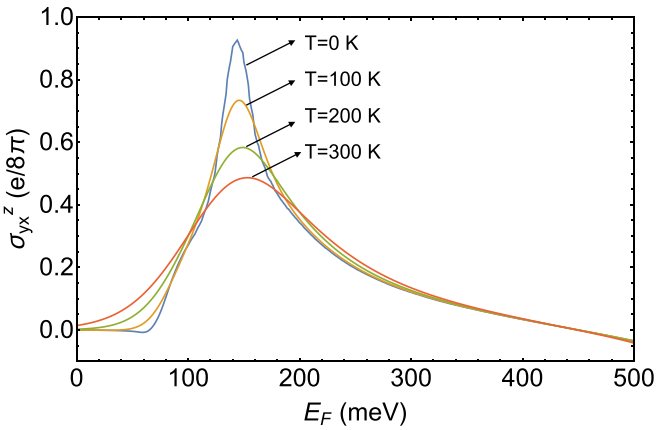

FIG. 7. Intrinsic SHC as a function of the Fermi level in $LaAlO_3/SrTiO_3$ 2DEGs strained by 1% along the [001] direction at various temperatures.

IV. CONCLUSIONS

We have developed a tight-binding Hamiltonian description of $LaAlO_3/SrTiO_3$ 2DEGs that accounts for strain via changing bond lengths and angles. Spin-orbit coupling and interfacial quantum confinement are included in the Hamiltonian. We calculated the intrinsic spin Hall conductivities as a function of the strain and chemical potential. Our results reveal a strong effect of the strain on the spin Hall conductivities as the doping level changes. We have also investigated the source of the large SHC by plotting the band-resolved densities of the Berry curvatures and identified "hot points" with exceptionally large Berry curvatures in the Brillouin zone. Strains along different directions mainly alter the intrinsic SHC through changes in the band structure and the band curvatures. Our calculations also show that the intrinsic SHC of strained systems is of the order of $(e/8\pi)$, so the effect is comparable to the values that were calculated from the Rashba spin-orbit interaction [35,36]. Exceptionally large, tunable spin Hall conductivities in these 2D systems with high carrier densities and large mobilities suggest that they could play a substantial role in developing spintronic devices.

ACKNOWLEDGMENTS

We acknowledge support from the Center for Emergent Materials, an NSF MRSEC under Award No. DMR-1420451, and an ARO MURI.

[1] H. Y. Hwang, Y. Iwasa, M. Kawasaki, B. Keimer, N. Nagaosa, and Y. Tokura, Nat. Mater. **11**, 103 (2012).

[2] A. Ohtomo and H. Y. Hwang, Nature **427**, 423 (2004).

[3] M. Vivek, M. O. Goerbig, and M. Gabay, Phys. Rev. B **95**, 165117 (2017).

[4] A. D. Caviglia, M. Gabay, S. Gariglio, N. Reyren, C. Cancellieri, and J.-M. Triscone, Phys. Rev. Lett. **104**, 126803 (2010).

[5] K. Narayanapillai, K. Gopinadhan, X. Qiu, A. Annadi, Ariando, T. Venkatesan, and H. Yang, Appl. Phys. Lett. **105**, 162405 (2014).

[6] J. Chakhalian, A. J. Millis, and J. Rondinelli, Nat. Mater. **11**, 92 (2012).

[7] M. Peña and J. L. G. Fierro, Chem. Rev. **101**, 1981 (2001).

[8] M.-J. Jin, S. Y. Moon, J. Park, V. Modepalli, J. Jo, S.-I. Kim, H. C. Koo, B.-C. Min, H.-W. Lee, S.-H. Baek *et al.*, Nano Lett. **17**, 36 (2017).

[9] E. Lesne, Y. Fu, S. Oyarzun, J. Rojas-Sánchez, D. C. Vaz, H. Naganuma, G. Sicoli, J.-P. Attané, M. Jamet, E. Jacquet *et al.*, Nat. Mater. **15**, 1261 (2016).

[10] N. Reyren, S. Thiel, A. D. Caviglia, L. Fitting Kourkoutis, G. Hammerl, C. Richter, C. W. Schneider, T. Kopp, A.-S. Rüetschi, D. Jaccard, M. Gabay, D. A. Muller, J.-M. Triscone, and J. Mannhart, Science **317**, 1196 (2007).

[11] S. Gariglio, N. Reyren, A. D. Caviglia, and J.-M. Triscone, J. Phys.: Condens. Matter **21**, 164213 (2009).

[12] M. Ben Shalom, M. Sachs, D. Rakhmilevitch, A. Palevski, and Y. Dagan, Phys. Rev. Lett. **104**, 126802 (2010).

[13] C. Şahin, G. Vignale, and M. E. Flatté, Phys. Rev. B **89**, 155402 (2014).

[14] R. Ohshima, Y. Ando, K. Matsuzaki, T. Susaki, M. Weiler, S. Klingler, H. Huebl, E. Shikoh, T. Shinjo, S. T. B. Goennenwein *et al.*, Nat. Mater. **16**, 609 (2017).

[15] Y. K. Kato, R. C. Myers, A. C. Gossard, and D. D. Awschalom, Science **306**, 1910 (2004).

[16] J. Wunderlich, B. Kaestner, J. Sinova, and T. Jungwirth, Phys. Rev. Lett. **94**, 047204 (2005).

[17] H. Kronmüller and S. Parkin (eds.), *Handbook of Magnetism and Advanced Magnetic Materials, Vol. 5: Spintronics and Magnetoelectronics* (Wiley, New York, 2007).

[18] S. Murakami, in *Advances in Solid State Physics* (Springer, Berlin, 2005), pp. 197–209.

[19] G. Vignale, J. Supercond. Novel Magn. **23**, 3 (2010).

[20] A. R. Mellnik, J. S. Lee, A. Richardella, J. L. Grab, P. J. Mintun, M. H. Fischer, A. Vaezi, A. Manchon, E.-A. Kim, N. Samarth, and D. C. Ralph, Nature **511**, 449 (2014).

[21] C. Şahin and M. E. Flatté, Phys. Rev. Lett. **114**, 107201 (2015).

[22] G. Y. Guo, S. Murakami, T.-W. Chen, and N. Nagaosa, Phys. Rev. Lett. **100**, 096401 (2008).

[23] B. Jalan, S. J. Allen, G. E. Beltz, P. Moetakef, and S. Stemmer, Appl. Phys. Lett. **98**, 132102 (2011).

[24] C. W. Bark, D. A. Felker, Y. Wang, Y. Zhang, H. W. Jang, C. M. Folkman, J. W. Park, S. H. Baek, H. Zhou, D. D. Fong, X. Q. Pan, E. Y. Tsymbal, M. S. Rzchowski, and C. B. Eom, Proc. Natl. Acad. Sci. USA **108**, 4720 (2011).

[25] Z. Huang, Z. Q. Liu, M. Yang, S. W. Zeng, A. Annadi, W. M. Lü, X. L. Tan, P. F. Chen, L. Sun, X. R. Wang *et al.*, Phys. Rev. B **90**, 125156 (2014).

[26] S. Nazir, M. Behtash, and K. Yang, RSC Adv. **5**, 15682 (2015).

[27] A. Antons, J. B. Neaton, K. M. Rabe, and D. Vanderbilt, Phys. Rev. B **71**, 024102 (2005).

[28] W. Wunderlich, H. Ohta, and K. Koumoto, Physica B: Condens. Matter **404**, 2202 (2009).

[29] Y. Wang, R. Ramaswamy, M. Motapothula, K. Narayanapillai, D. Zhu, J. Yu, T. Venkatesan, and H. Yang, Nano Lett. **17**, 7659 (2017).

[30] K. Ando, S. Takahashi, K. Harii, K. Sasage, J. Ieda, S. Maekawa, and E. Saitoh, Phys. Rev. Lett. **101**, 036601 (2008).

[31] M. Morota, Y. Niimi, K. Ohnishi, D. H. Wei, T. Tanaka, H. Kontani, T. Kimura, and Y. Otani, Phys. Rev. B **83**, 174405 (2011).

[32] V. Sih, R. C. Myers, Y. K. Kato, W. H. Lau, A. C. Gossard, and D. D. Awschalom, Nat. Phys. **1**, 31 (2005).

[33] G. Seibold, S. Caprara, M. Grilli, and R. Raimondi, Phys. Rev. Lett. **119**, 256801 (2017).

[34] N. Zhang, Y. Wang, J. Berakdar, and C. Jia, New J. Phys. **18**, 093034 (2016).

[35] J. Zhou, W.-Y. Shan, and D. Xiao, Phys. Rev. B **91**, 241302(R) (2015).

[36] L. X. Hayden, R. Raimondi, M. E. Flatté, and G. Vignale, Phys. Rev. B **88**, 075405 (2013).

[37] M. I. D'yakonov and V. I. Perel', Phys. Lett. A **35**, 459 (1971).

[38] J. E. Hirsch, Phys. Rev. Lett. **83**, 1834 (1999).

[39] S. Murakami, N. Nagaosa, and S.-C. Zhang, Science **301**, 1348 (2003).

[40] We consider a square confining potential to avoid the challenges of controlling the 2DEG with built-in electric fields. For example, in the low-density and weak confinement regime sometimes in self-consistent treatments higher subbands become depopulated [59,60] without changing the Fermi level [61]. We note that as long as the Kubo formula and band theory is valid the effect of localized disorder does not change the intrinsic SHC, as it is a full valence band property independent of the carrier scattering rates [21].

[41] M. Cardona, Phys. Rev. **140**, A651 (1965).

[42] A. H. Kahn and A. J. Leyendecker, Phys. Rev. **135**, A1321 (1964).

[43] S. Froyen and W. A. Harrison, Phys. Rev. B **20**, 2420 (1979).

[44] M. Jones and R. Albers, Phys. Rev. B **79**, 045107 (2009).

[45] T. M. Dunn, Trans. Faraday Soc. **57**, 1441 (1961).

[46] C. Fisk, C. Valdemoro, and S. Fraga, J. Chem. Phys. **48**, 2923 (1968).

[47] C. E. Moore, *Atomic Energy Levels. As Derived from the Analyses of Optical Spectra*, Vol. I (National Bureau of Standards, Gaithersburg, MD, 1949).

[48] D. J. Chadi, Phys. Rev. B **16**, 790 (1977).

[49] P. D. C. King, S. McKeown Walker, A. Tamai, A. de la Torre, T. Eknapakul, P. Buaphet, S.-K. Mo, W. Meevasana, M. S. Bahramy, and F. Baumberger, Nat. Commun. **5**, 3414 (2014).

[50] S. McKeown Walker, A. de la Torre, F. Y. Bruno, A. Tamai, T. K. Kim, M. Hoesch, M. Shi, M. S. Bahramy, P. D. C. King, and F. Baumberger, Phys. Rev. Lett. **113**, 177601 (2014).

[51] S. Gariglio, A. Fête, and J.-M. Triscone, J. Phys.: Condens. Matter **27**, 283201 (2015).

[52] L. F. Mattheiss, Phys. Rev. B **6**, 4740 (1972).

[53] E. Poindexter and A. A. Giardini, Phys. Rev. **110**, 1069 (1958).

[54] A. Janotti, D. Steiauf, and C. G. Van de Walle, Phys. Rev. B **84**, 201304(R) (2011).

[55] R. F. Berger, C. J. Fennie, and J. B. Neaton, Phys. Rev. Lett. **107**, 146804 (2011).

[56] Z. Zhong, Q. Zhang, and K. Held, Phys. Rev. B **88**, 125401 (2013).
[57] S. Nazir, M. Behtash, and K. Yang, Appl. Phys. Lett. **105**, 141602 (2014).
[58] X. Lin, C. W. Rischau, L. Buchauer, A. Jaoui, B. Fauqué, and K. Behnia, npj Quantum Mater. **2**, 41 (2017).
[59] C. Bell, S. Harashima, Y. Kozuka, M. Kim, B. G. Kim, Y. Hikita, and H. Y. Hwang, Phys. Rev. Lett. **103**, 226802 (2009).
[60] Z. Chen, H. Yuan, Y. Xie, D. Lu, H. Inoue, Y. Hikita, C. Bell, and H. Y. Hwang, Nano Lett. **16**, 6130 (2016).
[61] H. Boschker, C. Richter, E. Fillis-Tsirakis, C. W. Schneider, and J. Mannhart, Sci. Rep. **5**, 12309 (2015).